NOV 2009

Moon-based simulation of the Extreme Ultraviolet Radiation of the Earth's Plasmasphere

Fei He

Changchun Institute of Optics, Fine Mechanics and Physics, Chinese Academy of Sciences, Changchun, China

Graduated School of Chinese Academy of Sciences, Beijing, China

Xiaoxin Zhang

National Center for Space weather, China Meteorological Administration, Beijing, China

Bo Chen

Changchun Institute of Optics, Fine Mechanics and Physics, Chinese Academy of Sciences, Changchun, China

Mei-Ching Fok

NASA Goddard Space Flight Center, Greenbelt, MD, U.S.A

Abstract

The dynamic global core plasma model (DGCPM) is used in this study to calculate the He^+ density distribution of the Earth's plasmasphere and to investigate the configurations and 30.4 nm radiation properties of the plasmasphere viewed from the moon. Two storms observed by the IMAGE/EUV Imager are first used to validate the DGCPM, and then, the plasmaspheric EUV images are simulated from the moon using the DGCPM. It is found that the plasmaspheric 30.4 nm emission intensity viewed from the moon is 0.1~11.4 Rayleigh within the plasmapause and 0.02~0.1 Rayleigh outside, ~~and the plasmasphere is mainly located within 6.0 R_E.~~ The plasmaspheric shoulders and plumes are for the first time modeled from the moon with typical scale of 0.1 R_E. The plasmaspheric shoulders move toward the center of the image and the outer edge of the shoulders also move faster than the inner edges as IMAGE/EUV observations for the strong southward turning of the interplanetary magnetic field (IMF). It is demonstrated that the shapes and positions of the plumes of the plasmasphere dramatically depend on the solar wind and IMF conditions and geomagnetic conditions, ~~as well as imaging positions~~. Different plume configurations, such as, well-shaped along the central line of the image, well shaped around the plasmapause, and diffusive distributions outside the plasmapause are found in the simulations.

This investigation provides us with overall understanding on moon-based EUV imaging, and enables us to identify the plasmaspheric structures and evolution patterns in future moon-based EUV imaging.

Keywords:

The Earth's Plasmasphere, the Extreme Ultraviolet Radiation, the Moon-Based Imaging

1. Introduction

The Earth's plasmasphere is a torus of cold, dense plasma region that occupies roughly the same region of the inner magnetosphere as the ring current and radiation belts between 2.0 and 7.0 R_E (R_E is the Earth's radius). The typical electron density of plasmasphere is 10-10^4 cm^{-3}, with low temperature (less than 1-2 eV) compared with the rest of the magnetosphere (*Chiu et al.*, 1979; *Horwitz et al.*, 1986). H^+ is the dominant ion species in the plasmasphere. He^+ is the second abundant ion in the plasmasphere, comprising 5-10% of the total number density, and O^+ is the smaller population (usually less than 1%) originated from the ionosphere. The ratio between He^+ and H^+ changes with geomagnetic activities, ranging from 1% to 50% (*Farrugia et al.*, 1988; 1989), and the typical ratio between O^+ and H^+ is 0.05 to 0.10 (*Adrian et al.*, 2004). The ions of plasmasphere are all trapped on magnetic field lines and form a field aligned distribution. The outer boundary of the plasmasphere is called plasmapause, and this boundary is dynamic and highly structured during storm/substorm times. It is known that the plasmasphere is highly variable both spatially and temporally responding to changes in the solar wind and IMF conditions, exhibiting erosion and refilling processes, along with a high level of structure. The plasmasphere which strongly interacts with ionosphere, ring current and radiation belt is the core region of the inner magnetosphere, and its evolution process can affect the inner magnetospheric structure and near-Earth space environment.

One significant feature of the plasmasphere is to resonantly scatter the extreme ultraviolet (EUV) radiation of sun light (*Meier*, 1991), and the scattering intensity is proportional to ion density of the scattering point (*Sandel et al.*, 2000). Thus the best method to study the global dynamics of the plasmasphere is to optically image the radiation and then inverse the images to get plasmaspheric ion densities. The plasmaspheric EUV radiation mainly contains two lines: 30.4 nm by He^+ and 83.4 nm by O^+. The former is a line spectra with scattering rate between $1.8\sim3.4\times10^{-5}$ $photons\cdot ion^{-1}\cdot s^{-1}$ (*Garrido et al.*, 1994), and the latter is triplet spectra containing 9 lines with

scattering rate between 1.0~9.4×10^{-7} *photons·ion*$^{-1}$·s^{-1} (*Garrido et al.*, 1991). The advantage of selecting 30.4 nm emission also lies in that He^+ is the second abundant ion in the plasmasphere (~10%, but O^+ is less than 1%), and its distributions and dynamic properties can represent the overall plasmasphere. The 30.4 nm emission is a single line which is the strongest radiation of the plasmasphere; the magnetosphere is optically thin to the line (*Brandt*, 1961; *Meier and Weller*, 1972), and the background emissions can be neglected, thus the detection and calculation are simple and accurate. In addition, the response time of optical imaging is short in that one image can be shot in just several minutes. The EUV images are intuitively suitable for observation and research on the responses of plasmasphere to geomagnetic activities during storms and/or substorms, and also for space weather monitoring and forecasting.

The best way to monitor the plasma density and distribution evolution of the plasmasphere during geomagnetic activities is to optically image the radiation from the plasmasphere (*Carpenter*, 2004). However, optical imaging was not used to detect the plasmasphere for a long time due to the limitations of extremely low reflectivity of the optical elements in EUV wavelength, until the EUV multilayer and optical fabrication technologies experienced a great progress at the end of last century. The extreme ultraviolet (XUV) scanner onboard the Planet-B mission (*Yamamoto and Tsuruda*, 1998) carried out scanning imaging of the 30.4 nm emission of the plasmasphere during its travel to the Mars, and for the first time obtained the partial plasmaspheric 30.4 nm emission intensity distribution projected on the meridian plane (*Nakamura et al.*, 2000). However, the XUV has just imaged the partial plasmasphere during its near Earth parking orbit (from July 1998 to January 1999) because of the limitations of its operation period and FOV of scanner. The first overall EUV imaging of the plasmasphere was carried out by the EUV Imager onboard the Imager for IMAGE mission (*Burch*, 2000) from the apogean region of polar orbit (*Sandel et al.*, 2000) and many excellent results were obtained (*Sandel et al.*, 2001, 2003). The Telescope of Extreme Ultraviolet (TEX) onboard the SELENE mission (*Sasaki et al.*, 2003) carried out overall imaging of the plasmasphere from moon polar orbit (*Yoshikawa et al.*, 2008). Since the IMAGE/EUV and the SELENE/TEX worked on spin platforms and on polar orbits, the plasmaspheric evolution under geomagnetic storms and/or substorms has not been fully imaged.

However, these problems might be eliminated when imaging from the moon. The spin period of moon is equal to its revolution period which makes one side of the moon always orient to the

Earth. If an EUV imager is set on the surface of the moon, the FOV of the imager will always point to the Earth although there are small longitudinal and latitudinal disturbances, due to the elliptic orbit of the moon and the angle (5.15°) between the plane of lunar orbit and the ecliptic, which can be compensated by daily rotation of the imager. Thus the imager will image the plasmasphere continuously during a lunar day in one lunar period. The 60 R_E distance from the Earth to the moon makes the FOV of imager relatively small and easy to achieve, and the uniform spatial resolution can be realized all over the FOV at the same time. Combined with the high polar orbit EUV imager, the three dimensional plasmaspheric density distributions can be obtained by inversing the simultaneous images from the polar orbit and the moon. It is expected that the latitudinal properties and the flux tube configurations of the plasmasphere may be obtained through moon-based EUV imaging.

Since no overall plasmaspheric EUV images have been currently obtained from the moon, it is essential to simulate the moon-base EUV imaging of the Earth's plasmasphere. *Swift et al.* [1989] simulated the 83.4 emission by plasmaspheric O^+, and introduced the instrument needed. *Garrido et al.* [1994] simulated the He^+ 30.4 nm emission from the side view, though not as far as from the moon, the modeling principle is the same. For these two works, however, their spatial resolutions were limited by their density models used. In this investigation, the DGCPM is used to study the global structure of the plasmasphere evolutions viewed from the moon.

In this paper, the DGCPM used to construct the three dimensional plasmasphere density will be briefly introduced first in Section 2, and then validation of the model will be carried out by comparing the simulated plasmaspheric images with IMAGE observations in Section 3. In Section 4, we will study the method of imaging the plasmasphere from the lunar orbit, analyze its feasibility, and investigate the storm time plasmasphere evolutions viewed from the moon especially the evolution of shoulders and plumes. Finally, discussion and summary will be given in Section 5.

2. Simulation Approach

To simulate the 30.4 nm emission, three dimensional spatial distributions of the plasmaspheric He^+ density must be calculated first. The DGCPM used in this study was established by *Ober et al.* [1997] and the principle of the model will be briefly introduced here. It is assumed that the density along a magnetic flux tube is a constant and its density is determined by the flux in (dayside

ionosphere upward flux) or out (nightside downward flux) of the tube at the ionosphere. The model solves the following continuity equation (*Chen and Wolf*, 1972; *Rasmussen et al.*, 1993):

$$\frac{D_{\perp}N}{Dt} = \frac{F_n}{B_{ni}} + \frac{F_s}{B_{si}} \tag{1}$$

where $D_{\perp}/Dt$ is the convection derivation in the moving frame ($E \times B$) of the flux tube, N is the total ion content per unit flux, F_s and F_n are the flux in or out the flux tube at the northern and southern ionospheres, B_{ni} and B_{si} are the magnetic fields at the northern and southern ionospheric foot points of the flux tube respectively. Here the magnetic field pattern and electric field pattern should be specified in the plasmaspheric region. Empirical models are adopted since there is no way of measuring the global magnetic field and electric field pattern at present. The magnetic field models used in our calculations are the International Geomagnetic Reference Field (IGRF) model and Tsyganenko model (*Tsyganenko et al.*, 2005). The convection electric field pattern in the plasmasphere region is specified by the cross polar cap potential from Weimer empirical model (*Weimer*, 2005) and then the potential distribution is mapped into the plasmasphere along magnetic field lines (assuming equipotential magnetic field lines).

Numerical method can be used to solve this first order hyperbolic partial differential equation (1), and the plasmaspheric density distribution at random time can be derived. When simulating the plasmaspheric evolution, the magnetic flux tubes are initialed with saturated density (*Carpenter and Anderson*, 1992) and then convected for 5-6 days to reach an equilibrium stage under weak solar wind conditions. Then the model is solar windtched to a strong convection so as to investigate the plasmaspheric structures and evolutions during storm times.

The initial plasmaspheric He^+ density can be obtained from *Craven et al.* [1997], and the ratio between the density of He^+ and H^+ can be given by (*Gallagher et al.*, 2000)

$$\log_{10}\left(\frac{n_{He}}{n_H}\right) = -1.541 - 0.176r + 8.557\times10^{-3}P - 1.458\times10^{-5}P^2. \tag{2}$$

Here n_{He} and n_H represent the number densities of He^+ and H^+ respectively, r is the distance from the Earth center in R_E and P is the mean value of daily 10.7 cm solar flux ($F_{10.7}$) and its 81-day averaged value ($F_{10.7A}$). The values of $F_{10.7}$ and $F_{10.7A}$ can be obtained from real time observation or model calculation (*Richard et al.*, 1994).

T96, T04??

177 Tsyganenko model is used to construct the meridian plane density for simplicity. Figure 1 shows
178 an exampled density distribution in three different planes.

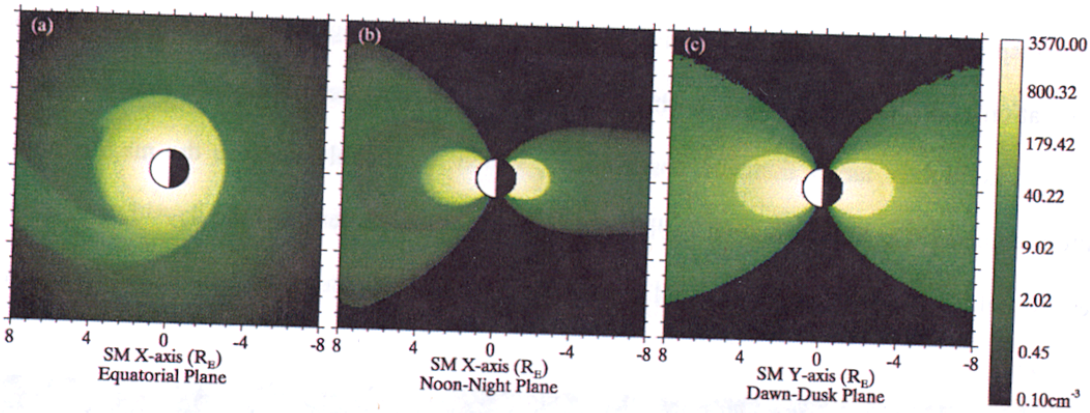

179

180 **Figure 1.** Plasmasphere densities from the DGCPM at UT08:46 24 May 2000: (a) for equatorial
181 plane; (b) for dawn-dusk meridian plane; and (c) for noon-night meridian plane. The log-scaled
182 color bar is shown at the right in cm^{-3}.

183 **3.2 Storm on 24 May 2000**

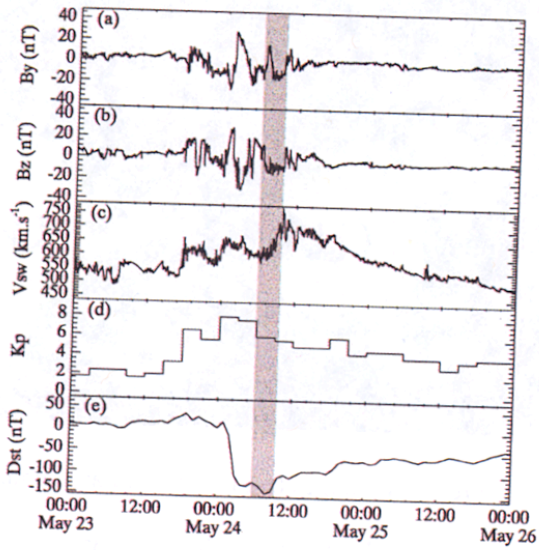

184

185 **Figure 2.** Solar wind and IMF parameters and geomagnetic *Kp* and *Dst* indices on 24 May 2000.

186 The shaded solar wind and IMF parameters and geomagnetic *Kp* and *Dst* indices of a storm on
187 24 May 2000 (as shown in Figure 2) are employed in the DGCPM to obtain the plasmaspheric
188 density distributions and simulate the EUV images. During this period, the IMF has a strong
189 southward turning, and the solar wind velocity increases continuously. This results in a peak *Kp*
190 value of 7+ and a *Dst* minimum of -150 nT, corresponding to the turning stage of main phase and
191 recovery phase of the storm. Both the IMAGE/EUV images (Figure 3a-3c) and the simulated
192 images (Figure 3d-3f) in Figure3 are projected onto the SM equatorial plane, in which the counts

of the EUV instruments are converted to emission intensity (Rayleigh) using the method involved in *Gallagher et al.* [2005]. During this stage, the plasmasphere is eroded by the strong magnetospheric convection and shrinks inward, causing the nightside plasmapause in both observation and DGCPM images to shrink to about 3.0 R_E, while the dayside plasmapause of DGCPM is slightly larger than the observations, which is probably because the magnetic field pattern embedded in the simulation is different from the actual pattern and the dayside convection electric field is stronger than the actual electric field, causing the sunward convection to become stronger.

Any comment on the difference between IMAGE/EUV images and the calculated images?

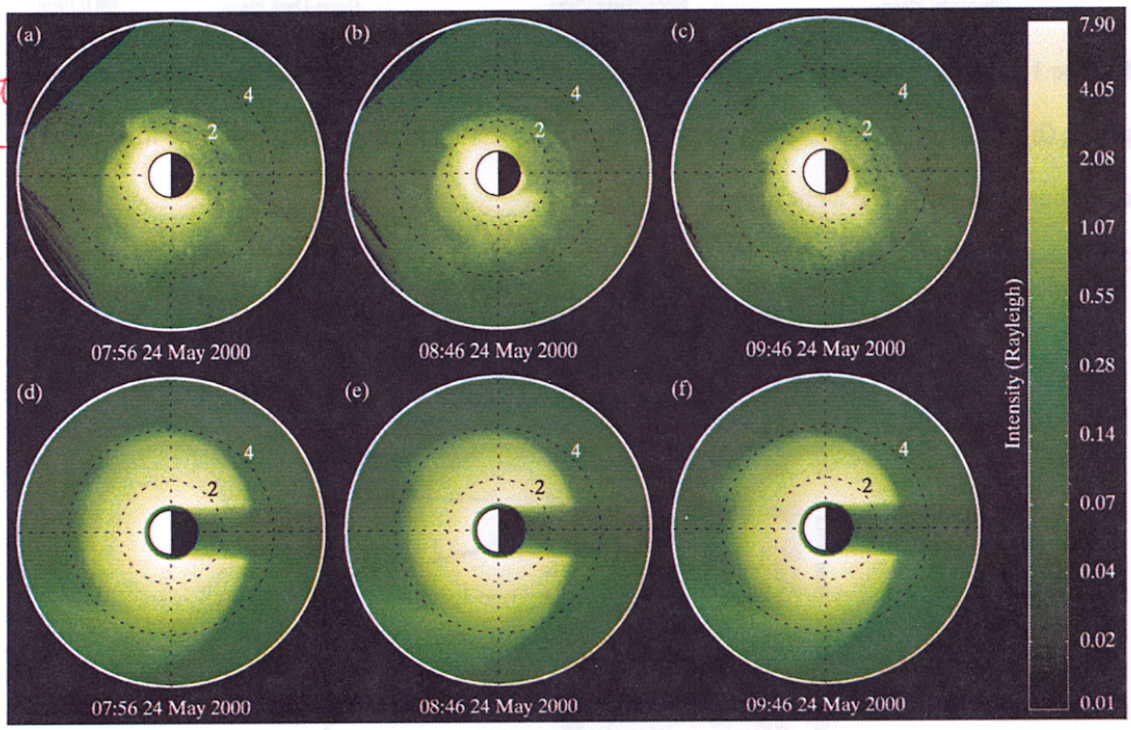

Figure 3. Comparison of IMAGE/EUV images (a-c) with simulated images (d-f) at UT=0756, 0846, and 0946 on 24 May 2000. In the EUV images the views are over the North Pole and the images are projected to the SM equatorial plane with the Sun to the left. The Earth radii represented by the dashed circles are shown near the circles in R_E.

The width of the plume becomes narrow and the shoulder turns toward noon for the strong southward turning of the IMF as shown in Figure 3a-3c. In the simulation, when the solar wind and IMF conditions enhance, the strong convection electric field shields the inner magnetosphere (*Goldstein, et al.*, 2002), and the shoulder is formed and rotates toward noon as observed by IMAGE. The rotating speed of the shoulder in the simulation is consistent with the observations. It is also modeled that the outer edge of the shoulder rotates faster than the inner edge.

3.3 Storm on 26 June 2000

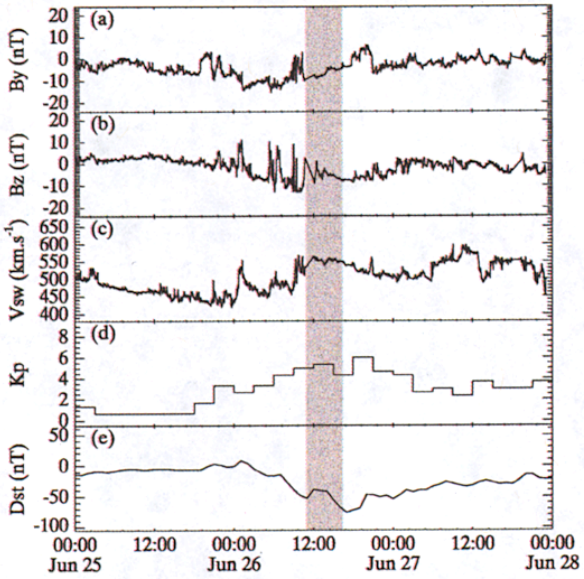

Figure 4. Solar wind and IMF parameters and geomagnetic *Kp* and *Dst* indices on 26 June 2000.

The magnetic storm on 26 June 2000 in Figure 4 is weaker than that on 24 May as shown in Figure 2. During the shaded period, the IMF also has a south-ward turning but does not change as suddenly as 24 May storm, the solar wind velocity maintains a relatively high level though it begins to decrease, and the *Kp* and *Dst* indices both maintain a medium level. During this period, the plasmasphere is eroded by the relatively strong magnetospheric convection and shrinks continuously, and the plasmapause shrinks to about 3.0 R_E. The plume narrows and rotates toward dusk as shown in Figures 5a-5c. ~~That~~ There are no shoulder is formed in this case reveals that the solar wind convection is not strong enough to shield the inner magnetosphere. Figures 5d-5f represents the results of DGCPM deployed with the shaded solar wind and IMF parameters in Figure 4. The simulation results are approximately consistent with the observations. Both the dayside and nightside plasmapauses kept at 3.0 R_E are consistent with the observations.

It is shown from both Figure 3 and Figure 5 that the radial decreasing tendency of the emission intensity within the plasmapause calculated from DGCPM is slower than that of IMAGE observations, whereas the He^+ densities at higher latitude are greater than at lower latitude in actual situations (*Nsumei et al.*, 2003). There are no bright horseshoe-shaped regions at about 1.0 R_E in our simulations since the ionospheric He 58.4 nm, O^+ 83.4 nm and 53.9 nm and other emissions are not considered.

showed in Figure 2. In Figure 6, the vertical direction represents the *Y*-axis in frame of the camera which is almost parallel to the *Z*-axis of *SM* coordinates system (since the angle between the ecliptic and lunar orbit is just 5.15°), the horizontal direction represents the *X*-axis in frame of the camera assuming that the normal of the camera is the *Z*-axis in frame of the camera. The density at UT08:46 on 24 May 2000 is used to construct the EUV images and the corresponding intensity viewed from polar orbit is shown in Figure 3e.

The modeled He^+ 30.4 nm emission intensity from the main body of the plasmasphere (within the plasmapause) shown in Figure 6 is 0.1-11.4 Rayleigh which is consistent with early sounding rockets measurements of 0.1~10 Rayleigh (*Ogawa and Tohmatsu*, 1971; *Paresce et al.*, 1973), consistent with simulated intensity of 0.1~15 Rayleigh (*Roelof et al.*, 1992) and with the measurements of 0.1~7 Rayleigh done by Planet-B mission (*Nakamura et al.*, 2000). The intensity in the plasmasphere trough region outside the plasmapause is approximately 0.02~0.1 Rayleigh. The He^+ density beyond the plasmapause is quasi-stable, with a density of 0.2-2.0 cm^{-3} according to DGCPM and GEOTAIL measurements (*Matsui et al.*, 1999). The corresponding column integrated intensity is 0.026-0.13 Rayleigh which is consistent with our simulation.

Well-shaped plasmaspheric shoulders and plumes are modeled from the moon for the first time. The shape and position of the plumes change dramatically with modeling positions (marked by white arrows in Figure 6) since the LOS directions and the projection directions are different. Because of the shielding and overlapping effect of the LOS integration, the closer the moon is to its dawn or dusk, the less significant the plumes are in the images. The wrapped plumes shown in Figure 3 appear to surround the main body of the plasmasphere in side views (see Figure 6c-6e). The plasmaspheric shoulders appear only in images of Figure 6c-6e (see the dashed rectangle regions). The shoulders are not apparent at other positions because of the line overlapping effect. The spatial size of the shoulder is approximately 0.3 R_E. In addition, viewed from the moon, the plasmaspheric shoulders are not as strong as that of polar orbit because of the shielding of the main body of the plasmasphere and the plume.

Actually shoulders are hardly seen from the moon.

When the imager is located at position (*c*), the temporal evolution of the EUV images for 26 June 2000 storm is shown in Figure 10. The azimuthal direction of the plume on the equatorial plane is nearly parallel to the imager-Earth line in this case. The plumes in the images are all along the vertical directions. As the plumes become narrow in azimuth on the equatorial plane, the plumes in the images also narrow. The equatorial plane plasmasphere are eroded during the period from UT 12:16 to 16:11, which can also be seen from Figure 10.

4.3 Identifying plasmaspheric features from EUV images

EUV Images from the side views can help us to analyze the real time images of a EUV camera. Firstly, we can ~~know where~~ identify the location of the shoulders ~~may locate.~~ It is know from our simulations that the shoulders should appear in the low or parts of the images and move to the center of the images as time ~~going~~ goes on. Secondly, the direction and shape of plumes can be identified from real time images. For example, (i) the plumes locate at center of the image and extend directly along the vertical direction (see Figure 7c, Figure 10), then we could judge that the azimuthal direction of plumes on the equatorial plane is the same as the normal of the imager. We would also conclude that if the plumes in the EUV images have no wrapping then the plumes on the equatorial plane will extend directly from the main plasmasphere without wrapping; (ii) the plumes locate at the right or left edge of the images and are attached to the main body of the plasmasphere with a diffusive distribution (see Figure 9), and then the direction of plumes on the equatorial plane may be perpendicular to the normal of the imager; (iii) The plumes locate at the right or left edge of the images and encircle the main body of the plasmasphere (see Figure 6c-6e, Figure 8), and then the plumes may be wrapped on equatorial plane; (iv) The plumes move toward one direction in the images (see Figure 8 and Figure 10), revealing that the plumes are rotating on the equatorial plane.

5. Conclusions

Optically imaging the plasmasphere from different perspectives provides us with overall understanding of the evolution of the plasmasphere during geomagnetic activities. The moon-based EUV imaging is an excellent approach to study the latitudinal and azimuthal dynamics of the plasmasphere by inverting EUV intensities to helium ion densities, (possibly) combined with EUV images obtained from polar views. We have used the DGCPM to simulate the structural and radiation properties of the plasmasphere, compared them with the results of IMAGE mission and calculated the plasmaspheric EUV radiation intensity from different

observation positions from the lunar orbit. The main simulation results are as follows:

1. The 30.4nm radiation intensity of the plasmasphere imaging from the moon is 0.1~11.4 Rayleigh within the plasmapause and 0.02~0.1 Rayleigh beyond the plasmasphere. These values are greater than intensities viewed from the polar orbit because the column integration range from the moon is larger than that of the polar orbit. The EUV emission from the airglow of the Earth is not considered in this study and will be investigated in future work.

2. Viewed from the moon, the plasmasphere is mainly located within 6.0 R_E. The typical scale sizes of plasmapause, shoulder and plume are 0.1 R_E. The average radial velocity of erosion or refilling of the plasmasphere during storm time is approximately 0.1 R_E/min (*Goldstein et al.*, 2003; *Murakami et al.*, 2007). Thus we conclude that a camera with FOV of 15°, spatial resolution of 0.1 R_E (angular resolution of 0.095°) and temporal resolution of 10 min or better is required in moon-based EUV imaging.

3. The EUV images of the plasmaspheric shoulder and plume are for the first time modeled in the views from the moon. The evolutions of the plasmaspheric structures are greatly different from that viewed from polar orbit. Projected on the magnetic equatorial plane, the plasmasphere is approximately circularly shaped with some asymmetric structures; however, it is approximately oval-shaped when projected on meridian plane. The plumes rotate, become narrow and wrap on the equatorial plane, but their shapes and positions in the polar images do not change much with imaging positions. In the case of moon-based imaging, however, their shapes and positions in the images change dramatically with imaging positions. They may be in the left, right or center of the images, and they may be diffusive or well shaped. The shoulders experience different evolution patterns with polar orbit too. The shoulders rotate around the plasmapause on the equatorial plane toward noon, while it moves almost horizontally toward the center of the moon-based images. The identification method of shoulders and plumes is introduced at the end of section 4.

This investigation provides us with a clear overall understanding on moon-bases EUV imaging. The plasmaspheric features simulated in this work will be identified in the observations of the moon-based EUV camera in the Second Phase of Chinese Lunar Exploration Program which will be implemented in 2012. Investigations in this study will also help us to analyze plasmaspheric structures in future moon-based EUV imaging and the modeled results can be used as initial solutions to do image inversions in future work.

the shape of the plume viewed from the moon & from the Earth are different. However, what is cool is if additional feature that we can see from the Moon but not from the Earth. Is there any feature of this kind?